Topological phase transitions in functional brain networks

Fernando A. N. Santos,[1,*] Ernesto P. Raposo,[2] Maurício D. Coutinho-Filho,[2] Mauro Copelli,[2] Cornelis J. Stam,[3] and Linda Douw[4]

[1]*Departamento de Matemática, Universidade Federal de Pernambuco, 50670-901 Recife, PE, Brazil and Laboratório de Física Teórica e Computacional, Departamento de Física, Universidade Federal de Pernambuco, 50670-901 Recife, PE, Brazil*

[2]*Laboratório de Física Teórica e Computacional, Departamento de Física, Universidade Federal de Pernambuco, 50670-901 Recife, PE, Brazil*

[3]*Department of Clinical Neurophysiology and MEG Center, Amsterdam UMC, Vrije Universiteit Amsterdam, Amsterdam Neuroscience, 1081 HV, Amsterdam, The Netherlands*

[4]*Department of Anatomy & Neurosciences, Amsterdam UMC, Vrije Universiteit Amsterdam, Amsterdam Neuroscience, 1081 HZ, Amsterdam, The Netherlands*

(Received 21 December 2018; revised manuscript received 4 July 2019; published 30 September 2019)

Functional brain networks are often constructed by quantifying correlations between time series of activity of brain regions. Their topological structure includes nodes, edges, triangles, and even higher-dimensional objects. Topological data analysis (TDA) is the emerging framework to process data sets under this perspective. In parallel, topology has proven essential for understanding fundamental questions in physics. Here we report the discovery of topological phase transitions in functional brain networks by merging concepts from TDA, topology, geometry, physics, and network theory. We show that topological phase transitions occur when the Euler entropy has a singularity, which remarkably coincides with the emergence of multidimensional topological holes in the brain network. The geometric nature of the transitions can be interpreted, under certain hypotheses, as an extension of percolation to high-dimensional objects. Due to the universal character of phase transitions and noise robustness of TDA, our findings open perspectives toward establishing reliable topological and geometrical markers for group and possibly individual differences in functional brain network organization.

DOI: 10.1103/PhysRevE.100.032414

I. INTRODUCTION

Topology aims to describe global properties of a system that are preserved under continuous deformations and are independent of specific coordinates, while differential geometry is usually associated with the system's local features [1]. As they relate to the fundamental understanding of how the world around us is intrinsically structured, topology and differential geometry have had a great impact on physics [2,3], materials science [4], biology [5], and complex systems [6], to name a few. Importantly, topology has provided [7–13] strong arguments toward associating phase transitions with major topological changes in the configuration space of some model systems in theoretical physics. More recently, topology has also started to play a relevant role in describing global properties of real-world, data-driven systems [14]. This emergent research field is called topological data analysis (TDA) [15,16].

In parallel to these conceptual and theoretical advances, the topology of complex networks and their dynamics have become an important field in their own right [17,18]. The diversity of such networks ranges from the internet to climate dynamics, genomic, brain and social networks [17,18]. In this context, the application of ideas of TDA to the study of complex networks has been considered [6], and there are significant concepts still to be explored in the bridge between theoretical results in algebraic topology of random simplicial complexes [19], theoretical physics and complex systems [20,21]. Many of these networks are based on intrinsic correlations or similarities relations among their constituent parts. For instance, functional brain networks are often constructed by quantifying pairwise correlations between time series of brain activity recorded from different regions in an atlas spanning the entire brain [18].

Here we report the discovery of topological phase transitions in functional brain networks. We merge concepts of TDA, topology, geometry, physics, and high-dimensional network theory to describe the topological evolution of complex networks, such as the brain network, as a function of their intrinsic correlation level. We consider that the complex network is related [15,22] to a multidimensional structure, called the simplicial complex, and that a topological invariant (the Euler characteristic, see below) suffices to characterize the sequence of topological phase transitions in the complex network. The simplicial complex associated with a network is constituted by its set of nodes, edges, triangles, tetrahedrons, and higher-dimensional structures [15,22]. A simplicial complex is therefore a multidimensional structure that can be extracted, for instance, from a functional brain network. Our interdisciplinary approach was able to transpose recent rigorous results concerning phase transitions in simplicial complexes [19,23] to real-world networks, particularly functional brain networks.

*fansantos@dmat.ufpe.br

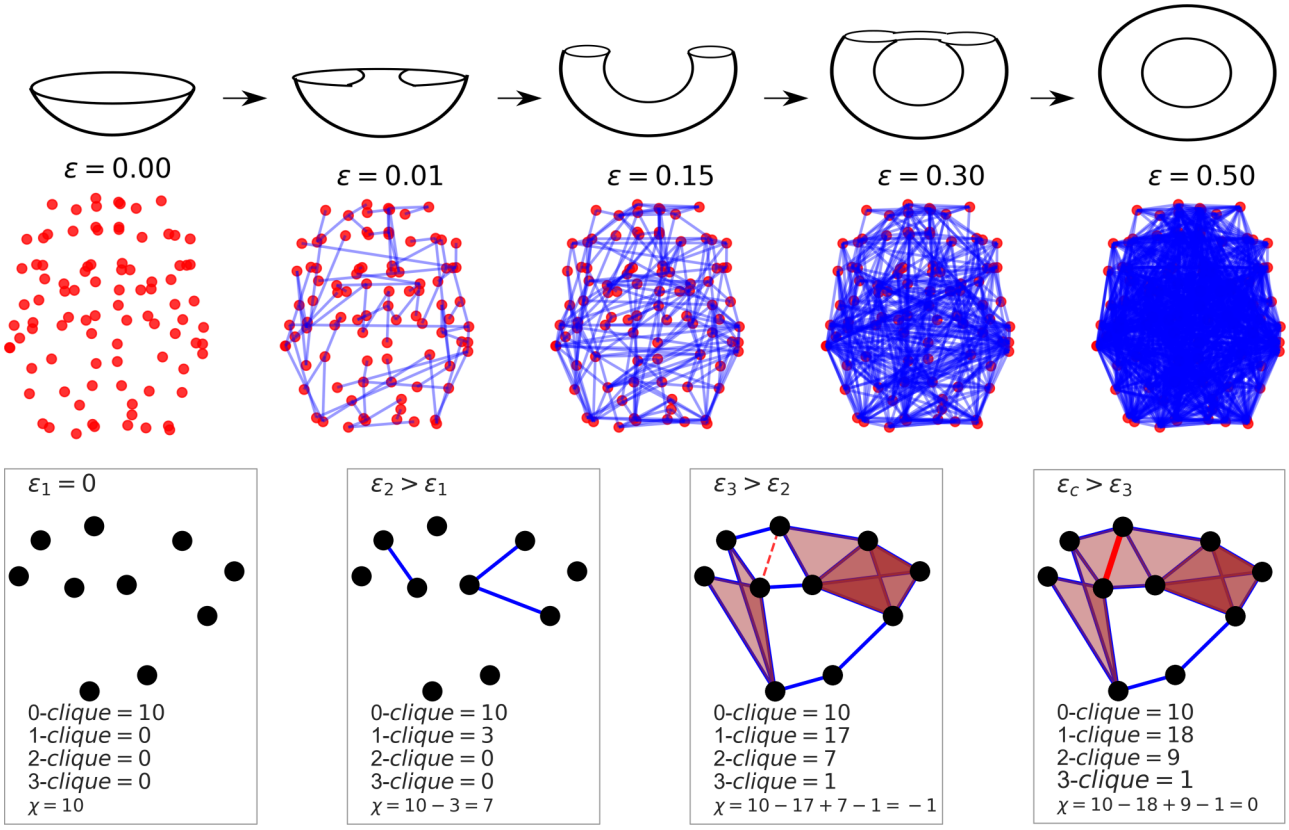

FIG. 1. Illustration of the filtration process in a functional brain network and analogy with the level sets of a torus. The middle panel shows regions (red dots) of an individual's brain from the VUmc data set. In the filtration process, a functional brain network is built for each value of the correlation threshold $\varepsilon \in [0, 1]$ by assigning an edge linking two brain regions if their normalized correlation level is larger than $1 - \varepsilon$. Therefore, a brain network with no links corresponds to $\varepsilon = 0$, whereas a fully connected structure arises for $\varepsilon = 1$. As ε is enhanced, new edges are gradually attached, thus changing the topology of the brain network, which becomes increasingly denser and harder to analyze. This process is analogous to the evolution of level sets in a surface, illustrated as a torus in the top panel, with the increasing of the height parameter level. In this analogy, a topological change takes place in the surface when the level set reaches up a value that delimits cross-section configurations with one and two circles. Topological invariants are able to track these changes in the evolution of both surfaces and networks. Each network has an associated topological structure, its simplicial complex, constituted by its nodes ($k = 1$), edges ($k = 2$), triangles ($k = 3$), tetrahedrons ($k = 4$), and higher $(k - 1)$-dimensional parts, the so-called k-cliques, as shown in the illustrative example of the bottom panel. The alternate sum of the numbers of k-cliques determines the Euler characteristic χ. A topological phase transition represents a major change in the network topology, occurring at the value of ε for which $\chi = 0$.

We establish a bridge between the above interdisciplinary formalisms by using correlation levels in functional brain networks just like one slices the energy levels in a Hamiltonian physical system [7,10,24–26] or the height function in Morse theory [27] and computational topology [15,22]. In a Hamiltonian physical system these topological changes occur as energy is increased, while in a functional brain network they emerge as the correlation threshold (or any other similarity measure) is varied. This puts the network simplicial complex on a similar footing to the configuration space of the Hamiltonian system dynamics, except for the very relevant gap that the underlying Hamiltonian function of actual complex systems is usually unknown and often inaccessible [28]. Under the intrinsic topological approach we propose here, the possibility emerges that this gap can be circumvented (at least partially), thus allowing for significant progress in network theory, even in the absence of a Hamiltonian description of the study system.

Some concepts from statistical physics present analogous topological counterparts, as discussed below. Such an analogy can be built by merging elements from TDA, physics, topology, differential geometry, and high-dimensional network theory to describe the topological evolution of networks that arise from intrinsic correlations in complex systems, including functional brain networks (see Fig. 1).

We apply our theoretical framework to Erdős-Rényi graphs [29], as well as to brain networks built from resting-state functional magnetic resonance imaging (rs-fMRI) connectivity data publicly available through the Human Connectome Project (HCP) [30,31] and from VU University Medical Center (VUmc, Amsterdam) [32]. In Erdős-Rényi graphs, the associated random network with uncorrelated links between nodes is exactly solvable [33] and the behavior of the Euler characteristic can be analytically understood. Moreover, the generalization of Erdős-Rényi graphs to the context of simplicial complexes was rigorously performed in Refs. [19,23,34].

Therefore, Erdős-Rényi graphs can serve as a reliable test ground system for our approach to brain networks. In both cases we find a sequence of topological phase transitions as a function of the linking probability in Erdős-Rényi graphs or the magnitude of intrinsic correlations from rs-fMRI measurements in functional brain networks. However, it is important to stress that the brain networks are shown here to have a remarkable local structure that is not displayed by Erdős-Rényi random networks.

The Euler characteristic [22] is a central quantity that we address in this work. Its history goes back to Plato [35]. Consider, for instance, a tetrahedron in three dimensions. It has $N = 4$ nodes, $E = 6$ edges, and $F = 4$ faces. Its Euler characteristic is $\chi = N - E + F = 2$. Exactly the same result for this alternate sum is obtained for a cube, an icosahedron, and any convex polyedron. In this sense, they are all homeomorphous to a sphere (a torus, however, yields a different result for χ due to the central hole). Thus, the Euler characteristic is an intrinsic property of a given object, which means that it does not depend on the particular parametrization of the object (see Fig. 1). The distinction between intrinsic and extrinsic properties of a system was introduced by Gauss [36] and made popular by Nash [37]. The Euler characteristic is also a topological invariant [22]. In the case of surfaces, this means that any two surfaces that can be transformed into each other by continuous deformations share the same Euler characteristic. For complex networks this concept is less intuitive, though one can say that two networks are topologically equivalent if a mapping between their representative graphs preserves their structure and, consequently, yields the same Euler characteristic.

The logarithm of the Euler characteristic was introduced as a potential link between thermodynamic entropy and topology [24], as evidenced in phase transitions in some exactly solvable physical models [7,8,24–26]. It was also used as a starting point for defining the entropy of the system in the context of the topological analysis of nuclear pasta phases [38]. In addition, theorems exploring the link between topology and phase transitions have been proposed [39], resulting in a general expression for the microcanonical entropy with an explicit topological contribution [7,40,41], recently extended to the thermodynamic limit [11]. Moreover, the Euler characteristic can be also interpreted as a measure [42], which allowed the definition of microcanonical thermodynamic averages using Morse indexes [10], in analogy with the work by Witten [43,44]. By doing so, the Euler entropy was proven to be topological equivalent to the Boltzmann entropy for exactly solvable classical interacting spin models [10].

From the above considerations, it will prove rewarding to explore here the topological phase transitions that take place in functional brain networks using the Euler characteristic. The robustness of our results is corroborated by the computation of another set of topological invariants called Betti numbers [22], which are associated with the number of multidimensional topological holes in the network, and therefore also with the organization of the functional brain network [45]. Although this approach is original for brain networks and complex systems in general, our work also finds support in recent rigorous results concerning the distribution of Betti numbers in random simplicial complexes [19,23].

We remark that the TDA framework is able to spatially locate the brain regions that participate most in the connected structures of the functional brain network [46]. With this information in hand, and based on a discrete version of a theorem relating differential geometry to topology [47,48], here we also provide a possible link between global (topological) and local (geometrical) properties of brain networks. This finding opens the perspective to advance in the quest for a link between local network structure and global functioning in brain networks [49,50].

The TDA framework is also particularly valuable since, on the one hand, the associated numerical analysis is rather robust against measurement noise [51], while it is also quite sensitive to characterize topological features of multidimensional structures, as recently suggested in Refs. [45,46,52].

Why is this relevant? Because phase transitions have a universal character by their own nature [53,54]. Therefore, in the same way that a substance that boils at 100 °C at sea level is very likely to be water, the critical points that locate the topological phase transitions in brain networks have the potential to be used as topological biomarkers. In this context, a change in the location pattern of the critical points of topological phase transitions in a brain network may signal a major change in the correlations among brain regions. It may therefore be fundamentally related to suboptimal brain functioning (see, e.g., Refs. [55–57]) and, in due time, can possibly become relevant to clinical neuroscience of neurological and psychiatric disorders [58].

Our topological approach may thus allow not only to discern novel features of brain organization relevant to human behavior, but also offers new avenues that can impact the investigation of individual differences in a nonbiased manner, such as in recent studies of task performance [59], differentiation between schizophrenia patients and healthy controls [60], and between attention-deficit hyperactivity disorder, autism spectrum disorder children, and pediatric control subjects [61].

II. RESULTS

The concept of the Euler characteristic of a surface was extended by Poincaré [62] to spaces of arbitrary dimensions and graphs as follows. A graph is a structure with nodes and edges. A k-clique is a subgraph with k all-to-all connected nodes. For example, each individual node is a 1-clique, each edge a 2-clique, each triangle a 3-clique, each tetrahedron a 4-clique, and so on. In other words, one can represent a k-clique as a $(k-1)$-dimensional object. In our notation, Poincaré's extension for the Euler characteristic χ of a graph is computed as an alternate sum of its numbers of k-cliques (see below).

A. Topological phase transitions in Erdős-Rényi graphs

Consider a set of N nodes (vertices or points). In an Erdős-Rényi graph [29] any two nodes are connected by a linking edge with probability p. Moreover, each edge is attached to the graph independently of every other edge. This implies that each node of an Erdős-Rényi graph is connected, on average, with $(N-1)p$ other nodes.

In a *random network* represented by an *Erdős-Rényi graph* [29], the uncorrelated connections between nodes occur with probability p. We can thus investigate the evolution of complex random networks (or Erdős-Rényi graphs) for fixed N nodes as a function of the probability parameter $p \in [0, 1]$. If $p = 0$, then no nodes are connected (empty graph), whereas if $p = 1$, then all nodes are fully linked to each other (complete graph). The random clique complex of the Erdős-Rényi graph is a simplicial complex in which all cliques are faces. The topology of the random clique complex was investigated rigorously in Ref. [19].

From the discussion above, in an Erdős-Rényi graph it is possible to identify subgraphs containing k-cliques with k all-to-all connected nodes (the simplicial complex) and then determine its Euler characteristic. The mean value of the Euler characteristic of Erdős-Rényi graphs with N nodes and linking probability p is exactly given by the alternate sum [33]

$$\langle \chi \rangle = \sum_{k=1}^{N} (-1)^{k+1} \binom{N}{k} p^{\binom{k}{2}} . \tag{1}$$

In the above expression, $\binom{N}{k} p^{\binom{k}{2}}$ is the mean number of k-cliques, since there are $\binom{k}{2} = k(k-1)/2$ links in a k-clique that occur with probability $p^{\binom{k}{2}}$. Also, the possible number of choices of k nodes from a total of N is $\binom{N}{k} = N!/(N-k)!k!$.

The Euler entropy [10] of the associated random network is obtained from

$$S_\chi = \ln |\langle \chi \rangle|. \tag{2}$$

As the linking probability is varied, when $\langle \chi \rangle = 0$ for a given value of p then the Euler entropy is singular, $S_\chi \to -\infty$. We shall see below that a zero of $\langle \chi \rangle$ and a singularity of S_χ are related to a significant topological change in the Erdős-Rényi graphs. In fact, a topological phase transition in a complex network takes place at the point where the Euler characteristic is null and the Euler entropy is singular. This statement finds support in the ubiquitous nonanalytical behavior of S_χ at the thermodynamic phase transitions across various physical systems [7,10,12,24–26,63,64]. Moreover, we show below that the behavior of a distinct set of topological invariants, the Betti numbers, also concurs to verify this assertion independently, a result that was rigorously reported for random simplicial complexes in Refs. [19,23,34].

Figure 2(a) displays the Euler entropy of Erdős-Rényi networks with $N = 50$ nodes as a function of the linking probability p, calculated from Eq. (1). We first notice the presence of several singularities in S_χ associated with the many zeros of the mean Euler characteristic given by a polynomial of degree $\binom{N}{2} = 50 \times 49/2 = 1475$, see Eq. (1). The observed sequence of topological phase transitions delimits several phases in the random networks, whose features can be unveiled by the analysis of the Betti numbers as follows.

The Betti number β_n counts the number of n-dimensional topological holes in the simplicial complex of a network [22]. For example, β_0 counts the number of connected components in the network or connected subgraphs in a graph, β_1 is the number of loops or cycles, β_2 represents the number of voids or cavities (like the one in the torus), and so on. We

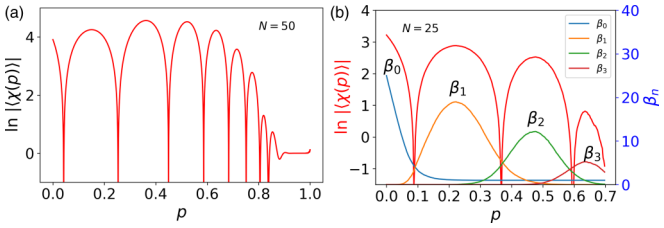

FIG. 2. Topological phase transitions in Erdős-Rényi random networks. (a) Euler entropy $S_\chi = \ln |\langle \chi \rangle|$ as a function of the probability p of connecting two nodes in an Erdős-Rényi graph with $N = 50$ nodes. S_χ was determined by Eq. (2), with the average Euler characteristic $\langle \chi \rangle$ exactly given [33] by Eq. (1). The zeros of $\langle \chi \rangle$ or the singularities $S_\chi \to -\infty$ locate the topological phase transitions in random networks. On the other hand, the topological phases are characterized by the Betti numbers β_n, shown in (b) for $N = 25$. Indeed, at each given phase one specific Betti number prevails, featuring which sort of n-dimensional topological hole predominates in the network structure. For example, for $N = 25$ and $0.09 \lesssim p \lesssim 0.36$ [between the first and second transitions in (b)] we note that β_1 (number of loops or cycles) is much larger than all other β_n's. The phase boundaries delimited by the dominant β_n's nicely agree with the loci of the topological phase transitions set by S_χ. As p increases, we find a sequence of transitions in which the dominant β_n varies (n is added by one unity) every time a transition point is crossed, thus signaling an important change in the topology of the Erdős-Rényi random network.

remark that the Euler characteristic can be also expressed as an alternate sum of Betti numbers [22].

In Fig. 2(b) we show the numerical results for β_n in the random clique complex with $N = 25$ vertices, indicating that the topological phase that sets in between the nth and $(n+1)$-th transitions corresponds very closely to the range in p where the Betti number β_n prevails. For instance, for $N = 25$ and $0.09 \lesssim p \lesssim 0.36$ (between the first and second transitions) we note that β_1 is much larger than all other β_n's. This means that loops ($n = 1$) are abundant in such random networks in this range of p. As p increases, we find a sequence of dominant Betti numbers β_n, starting from $n = 0$, that change (i.e., n is added by one unity) every time a topological phase transition is crossed. In other words, while the location of the transitions is determined by the singularities of the Euler entropy S_χ, the Betti numbers β_n characterize which kind of multidimensional hole prevails in each topological phase.

We remark that a rigorous investigation of the random clique complex in terms of the distribution of its homology groups and Betti numbers was performed in Ref. [19]. Here, however, we investigate the topological transitions by focusing on the zeros of the Euler characteristic or singularities of its logarithm (Euler entropy), based on long-term, ubiquitous counterparts and analogies with several branches of theoretical physics, with the added value that one can observe them experimentally in networks associated with complex systems. One important example comes from quantum field theory, in which the Witten index, a generalization of the partition function, is given by the manifold's Euler characteristic in the supersymmetric nonlinear sigma model [43]. Moreover, the zeros of the Euler characteristic correspond to the phase transitions in some discrete spin models, such as the Potts

model [12,65], random cluster [66], and Ising model [63,64], in the same fashion they also give rise to transitions in simplicial complexes in the present work. Further, singularities in the logarithm of the Euler characteristic (not necessarily its zeros) are also present at the phase transitions of some classical Hamiltonian systems [7,10,24–26].

Another interesting connection can be made with percolation theory. Indeed, the first transition in the sequence shown in Fig. 2(b) takes place at a value $p = p_c$ that nearly corresponds [23,29] to that of the usual percolation phase transition, which gives rise to the giant connected component of the Erdős-Rényi graph containing most of the network nodes. This finding is supported by recent rigorous results [19,23] from the distribution of Betti numbers that actually span all phase transitions, not only the first one, as well as from TDA of continuous percolation with disk structures [67]. In fact, the percolation transition in two-dimensional lattices [68] is known to occur in the vicinity of the only nontrivial zero of their Euler characteristic [69,70]. Moreover, it was also conjectured that the further zeros of the Euler characteristic are associated with continuous percolation transitions of higher-dimensional objects [70,71] and rigoroulsy analyzed for bounded regions in N-dimensional Euclidean spaces [13]. Since the lattice percolation problem involves the counting only of nodes, edges, and faces in the Euler characteristic [68,69,71], our results can further contribute to the detection of percolation transitions in higher-dimensional objects (triangles, tetrahedrons, etc.), a concept that was only very recently defined for complex systems [72]. Indeed, for systems where the distribution of Betti numbers in the limit $N \gg 1$ is concentrated in a finite interval, the percolation of k-cliques (or k-simplices) might occur in the vicinity of the critical point in which $\beta_k \approx \beta_{k+1}$ [19,23]. Therefore, in the thermodynamic limit and under conditions for the distribution of Betti numbers analogous to those in Refs. [19,23], the zeros of the Euler characteristic suffice to detect percolation transitions in higher-dimensional objects of the associated simplicial complex. For continuous systems, for example, the critical probability of percolation over a bounded region in an N-dimensional Euclidean space was estimated through the zeros of the Euler characteristc [13]. These results keep also an analogy with the so-called Yang-Lee theorem for phase transitions [73], in which the complex zeros of the partition function are related to thermodynamic phase transitions.

The Euler entropy has an interesting connection with information theory as well. In analogy with Shannon theorem [74], the Euler characteristic is the only nontrivial additive and multiplicative functional on simplicial complexes [75,76]. Links between the Euler characteristic and Shannon entropy were discussed rigorously in Ref. [77]. Moreover, the Euler characteristic can be also seen as a generalization of mutual information [78]. Yet, in a broader level, a homological version of information theory was proposed in Ref. [79] and, very recently, methods of TDA were transposed to information space [80], based on the isometry between Fisher information space and Euclidean space [81].

We can also comment on the order of the topological phase transitions in these complex networks. It is known [23] that the usual first percolation transition in Erdős-Rényi random graphs is of second order [53,54], in the sense that, e.g., the relative number of nodes linked by edges (2-cliques) in the giant component shifts without discontinuity from zero for $p < p_c$ to a non-null value for $p > p_c$. Nevertheless, the order of the subsequent transitions in Fig. 2(b) deserves further investigation. On the one hand, the similar logarithmic singular behavior of S_χ could suggest that the subsequent transitions are of second order as well. Notwithstanding, one cannot also discard a discontinuous first-order transition as observed in Ref. [23], in which the concept of the giant component was extended to higher-dimensional k-cliques structures, such as triangles ($k = 3$), tetrahedrons ($k = 4$), etc. A numerical study on the connectivity of ($k > 2$)-cliques and comparison with [23] may shed light on this point. Analogous arguments might also be applied to brain networks, as analyzed below.

B. Topological phase transitions in functional brain networks

Most real complex networks are not random networks or Erdős-Rényi graphs [17]. In particular, the connections between any two nodes (brain regions or voxels) in a functional brain network are not randomly established with probability p but are instead determined from the magnitude of their intrinsic correlations. One may thus ask whether topological phase transitions also occur in actual data-driven complex networks, such as functional brain networks.

To explore the relevance of the TDA framework to the analysis of functional brain networks, we consider two different rs-fMRI data sets. On the one hand, raw correlation matrices between $N = 177$ brain regions of 986 individuals were downloaded from the HCP data set [30,31], while, on the other hand, z-score values of correlations among $N = 92$ brain regions of 15 healthy individuals from the VUmc data set were also investigated [32]. These data sets represent two currently used approaches to perform graph analysis of rs-fMRI data (see *Methods*).

In the brain networks considered here, each node corresponds to a different region of the brain. Each individual is characterized by a $N \times N$ matrix C_{ij} of correlations between regions i and j, which is built from the time series obtained from rs-fMRI (see *Methods* for details). The filtration process in the TDA analysis involves the definition of a correlation threshold $\varepsilon \in [0, 1]$, so that, for the brain network of a given individual, two regions i and j are connected by an edge if the associated matrix element C_{ij} is such that $|C_{ij}| > 1 - \varepsilon$. This implies that for $\varepsilon = 1$ all regions in the brain are connected, while there are no connections if $\varepsilon = 0$. It is thus possible to follow the evolution of the functional brain network of each individual as a function of the correlation threshold level ε, in analogy to the previous analysis with p of the Erdős-Rényi random networks.

The Euler characteristic of the functional brain network of each individual is not given by Eq. (1), as in the case of random networks, but is expressed by the alternate sum of the numbers Cl_k of k-cliques present in the simplicial complex of the network for a given value of the correlation threshold ε [22],

$$\chi = \sum_{k=1}^{N} (-1)^{k+1} Cl_k(\varepsilon). \tag{3}$$

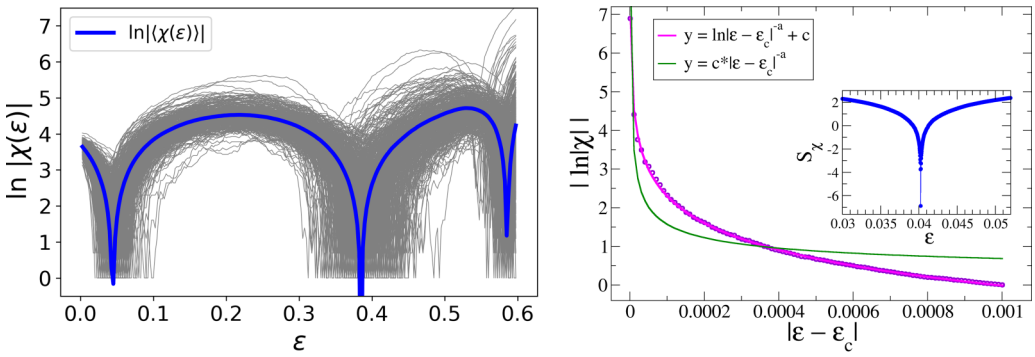

FIG. 3. Topological phase transitions in functional brain networks. (a) Euler entropy $S_\chi = \ln|\chi|$ as a function of the correlation threshold level ε of functional brain networks from the HCP data set. Each thin gray line represents an individual's brain network, whereas the thick blue line depicts their average. A sequence of three topological phase transitions in the brain networks is identified in this range of ε at the deepening points of S_χ (blue line). (b) A quite detailed analysis of S_χ near the first transition at $\varepsilon_c \approx 0.04$ was performed using steps $\Delta\varepsilon = 10^{-5}$ (inset), in contrast with $\Delta\varepsilon = 10^{-2}$ used in (a). The excellent fit (magenta line) to the data (blue circles) confirms the logarithmic singularity $S_\chi = \ln|\varepsilon - \varepsilon_c|^\alpha + c$, with c as a constant and best-fit exponent $\alpha = 1.004$ ($\alpha = 0.985$) as the transition is approached from below (above), in nice agreement with the theoretical prediction $\alpha = 1$. We also include for comparison the unsuccessful fit (green line) to the alternative form $S_\chi = c|\varepsilon - \varepsilon_c|^\alpha$.

The Euler entropy S_χ is thus obtained from χ as in Eq. (2).

Figure 3(a) shows the Euler entropy as a function of ε for the HCP data set. As discussed under *Methods*, the numerical computation of the numbers of k-cliques in brain networks becomes an increasingly (exponentially) difficult task as ε rises and more edges are progressively attached. This is actually an NP-complete problem, however, without a closed analytical expression available for the Euler characteristic of the brain network, such as Eq. (1) for the Erdős-Rényi graphs. This is in fact the reason we did not go beyond $\varepsilon = 0.60$ with steps $\Delta\varepsilon = 10^{-2}$ in Fig. 3(a), as data from only 420 of the 986 individuals in the HCP data set reached this value. Nevertheless, the Euler entropy averaged over all individuals (blue line) clearly shows the presence of three singularities in this range of ε, which correspond to the loci of the topological phase transitions taking place in these functional brain networks.

We comment that these singularities of S_χ resemble the singular cusp behavior of the Euler entropy reported at the phase transition of some physical systems [7,10]. Indeed, this finding is corroborated in Fig. 3(b) by the excellent fit of the data to the expression $S_\chi = \ln|\varepsilon - \varepsilon_c|^\alpha + c$, where c is a constant, as ε approaches the first transition point at $\varepsilon_c \approx 0.04$ with much narrower steps $\Delta\varepsilon = 10^{-5}$ for the whole HCP data set of 986 individuals. The inset of Fig. 3(b) shows the detailed behavior of S_χ in the critical region very close to ε_c [53,54]. The best-fit value of the exponent is $\alpha = 1.004$ ($\alpha = 0.985$) as the transition is approached from below (above). These results nicely agree with the prediction $\alpha = 1$ from the Euler characteristic written as a polynomial function with set of zeros $\{\varepsilon_{c,i}\}$, that is, $\chi = \prod_i(\varepsilon - \varepsilon_{c,i})$. By contrast, we also include in Fig. 3(b) the unsuccessful attempt to fit the alternative form $S_\chi = c|\varepsilon - \varepsilon_c|^\alpha$.

In order to provide further support to these results and additional characterization of the topological phases in the brain networks, we also calculate the Betti numbers β_n. Figure 4 presents results from both the HCP (top panel) and VUmc (bottom panel) data sets. In the former case we considered data from a subset of 712 individuals, which limited our analysis up to $\varepsilon = 0.50$.

The left and central plots of Fig. 4 show, respectively, the Euler entropy and the first three Betti numbers, $n = 0, 1, 2$. As evidenced in their average values displayed together in the right plots, in both data sets we notice a remarkable agreement between the transition points, determined by the singularities of S_χ, and the boundaries of the topological phases, characterized by each dominant β_n, as also observed theoretically in Ref. [23]. For instance, in the HCP data set the range between the first ($\varepsilon \approx 0.04$) and second ($\varepsilon \approx 0.39$) topological transitions nicely coincides with the phase in which β_1 is larger than both β_0 and β_2. In this regime, the brain network has plenty of one-dimensional topological holes (loops). In contrast, in the topological phase for $\varepsilon \gtrsim 0.39$ and up to the maximum ε reached in our study the dominant β_2 indicates the proliferation of voids or cavities in the more densely correlated network. Furthermore, the large value of β_0 below the first phase transition at $\varepsilon \approx 0.04$ implies a topological phase with substantial fractioning of the brain network into several disconnected components. In this sense, the first transition in Fig. 3(a) resembles the first percolation transition in the Erdős-Rényi random networks discussed above, below which the giant connected component cannot establish.

C. Connection between local network structure and brain function: From geometry to topology

A fundamental question that emerges in the present framework concerns the relation between the global (topological) features and local (geometric) properties of brain networks. Moreover, another rather important related issue is the understanding of the connection between network organization and brain function.

A key starting point in this direction might be the study of the individual nodes and their contribution to all-to-all

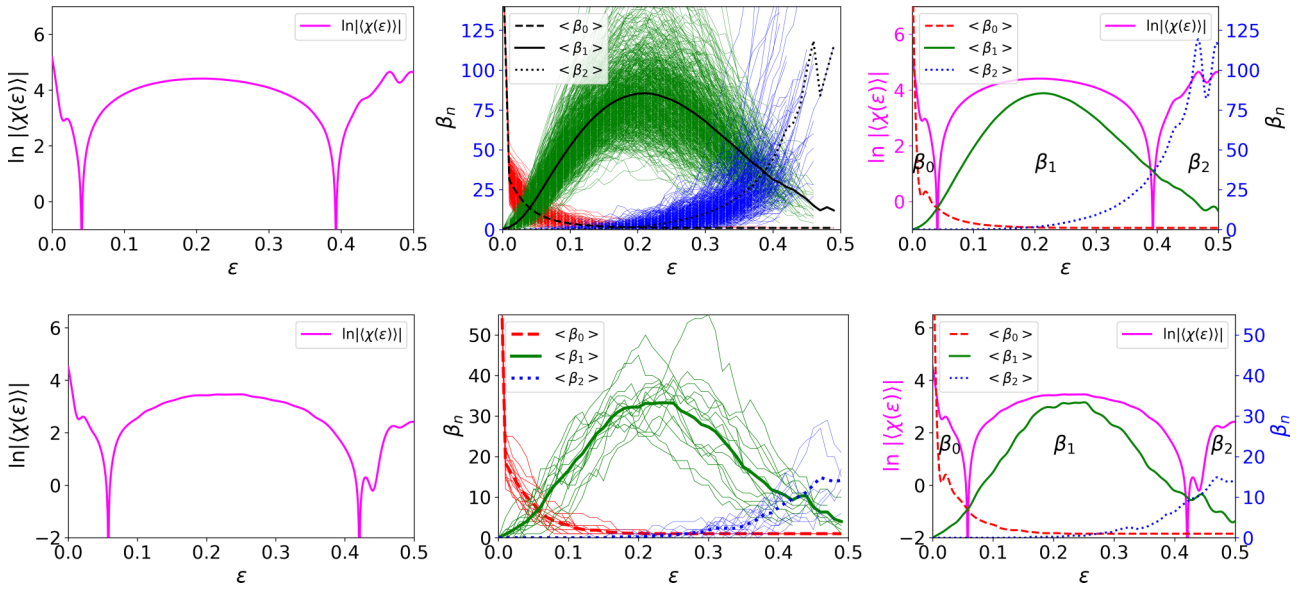

FIG. 4. Characterization of topological phases in functional brain networks from two different data sets. Euler entropy (left plots) and the three first Betti numbers (central plots) as a function of the correlation threshold ε of functional brain networks from the HCP (top panel) and VUmc (bottom panel) data sets. Each thin line in the central plots represents an individual's brain network, whereas thick lines depict their averages. As in Erdős-Rényi random networks, see Fig. 2, the right plots show a fine agreement between the phase boundaries, delimited by the dominant Betti numbers, and the loci of the topological phase transitions, set by S_χ. For values of ε below the first transition, where β_0 prevails, the brain network is characterized by a high fragmentation level, with the number of connected components larger than that of cycles, voids, etc. Between the first and second transitions, an important topological change takes place in the brain networks and the number of loops or cycles overcomes the number of connected components. After the second transition and up to the maximum threshold reached in our numerical analysis, β_2 becomes the dominant Betti number, indicating the proliferation of voids or cavities in the densely correlated functional brain networks, simultaneously with the vanishing of cycles.

connected k-cliques structures (triangles, tetrahedrons, etc.) that constitute the simplicial complex of the brain network. Indeed, the potential role of k-cliques for the link between structure and function has been recently addressed in the Blue Brain Project [49], where it was observed that groups of neurons are arranged in directed k-cliques that give rise to topological structures in up to 11 dimensions (i.e., maximum $k = 12$, see below) emerging in neocortical tissues.

In this context, a suitable local quantity to analyze is the participation rank of each node (brain region) in the k-cliques [46]. This quantity is denoted by $Cl_{ik}(\varepsilon)$ and counts the number of k-cliques in which node i participates for a given ε. Here we track the node participation rank in brain networks as a function of ε. Our approach thus differs from that of Ref. [46] in which a fixed correlation threshold was considered.

We start by illustrating in Fig. 5 the emergence, as ε increases, of 3-cliques only (triangles) in the functional brain network of an individual from the VUmc data set. We do not show results for values higher than $\varepsilon = 0.15$ because in this case the number of triangles rises considerably, hampering the visualization (see, e.g., the distribution of links in Fig. 1 for $\varepsilon > 0.15$). The color bars indicate the percentage of 3-cliques in which each node takes part. Remarkably, we notice that the distribution of the participation ranks in cliques is not homogeneous over the nodes, indicating a spontaneous differentiation between nodes as the correlation threshold raises. An html version of this figure is available in the Supplemental Material [82], in which it is possible to rotate the brain and identify the locations of the regions that participate most in the 3-cliques structures. We emphasize that an appropriate comparison between the cliques and cavities of fMRI brain networks with a null model was performed in Ref. [46].

Figure 6 depicts the node participation rank in *all* k-cliques (we do not draw triangles, tetrahedrons, etc., for clarity; see also the Supplemental Material [82]). We note that the nodes which participate in the largest numbers of k-cliques are ranked as the most important ones (according to the clique structure) [46]. We also observe that nodes with high participation seem to be similar to hubs defined on the basis of more conventional network measures [17,46], a point that should be explored in further studies, see, e.g., Ref. [83]. Since k-cliques are essential to compute topological quantities, such as the Euler characteristic and Betti numbers, the access to the distribution of node participation in k-cliques can contribute to the understanding, from a local perspective, of the topological phases and topological phase transitions in the brain network. Moreover, the identification of the spatial location of the main cycles and cavities in the brain network may also be relevant in the quest for a link between local structure and brain function, with potential applications to the local characterization of functional brain networks [46].

The connection between differential geometry and topology is also useful in this context. In differential geometry it is possible to define the concept of curvature at a given point of a surface essentially as a local measure of how the

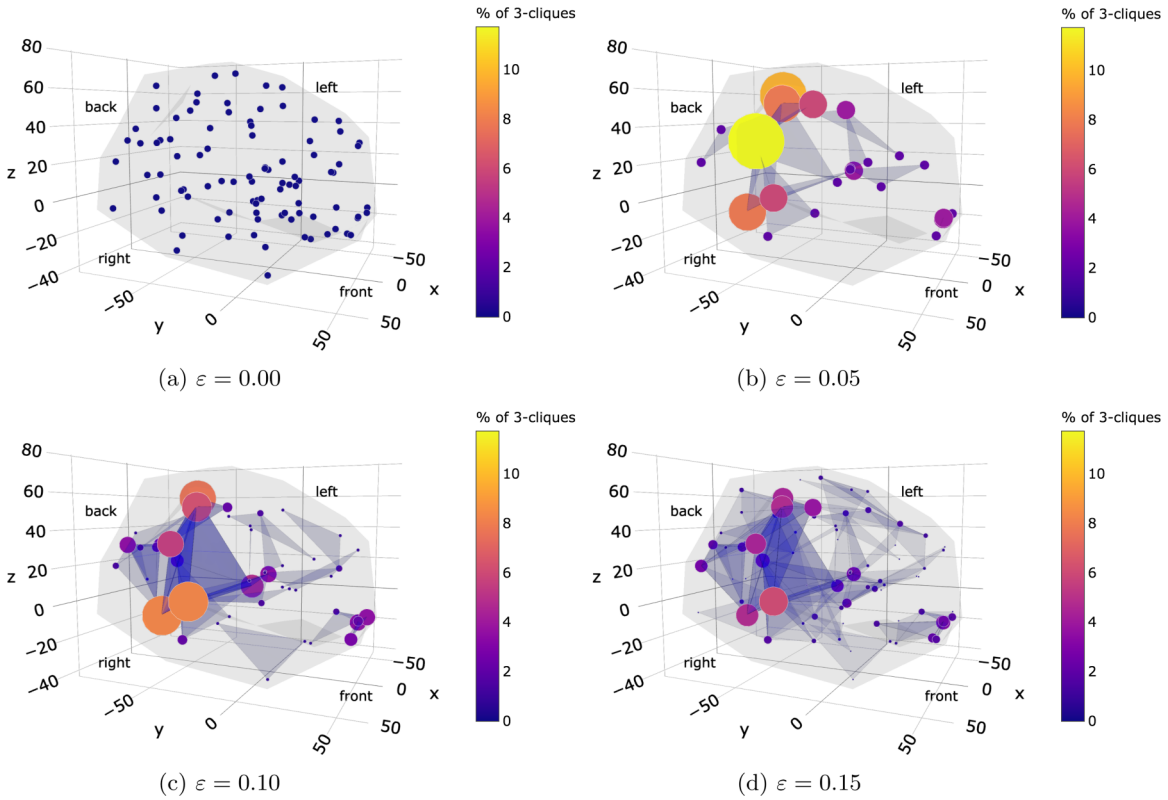

FIG. 5. Participation of brain regions in triangular structures in a typical functional brain network. Evolution with the correlation threshold ε of the normalized participation rank of each local brain region (small blue dots in (a)) in 3-cliques (triangles) structures in the brain network of a given individual from the VUmc data set. As ε increases, the color code and size of nodes, which are proportional to the participation in 3-cliques, indicate that an spontaneous differentiation of the role of distinct brain regions emerges in the functional brain network.

surface bends in distinct directions [1,36]. This concept can be extended to complex networks so that one possible definition of the network curvature κ_i at node i in terms of the node participation rank is given by [48]

$$\kappa_i = \sum_{k=1}^{k_{\max}} (-1)^{k+1} \frac{Cl_{ik}(\varepsilon)}{k}, \tag{4}$$

where $Cl_{i1} = 1$ since each node i participates in only one 1-clique (the node itself). Also, $k_{\max}$ represents the maximum number of nodes that are all-to-all connected in the network. Thus, since k all-to-all connected nodes form a $(k-1)$-dimensional object, as discussed above, then one can say that the simplicial complex of the network comprises topological structures in up to $k_{\max} - 1$ dimensions. We also observe that Eq. (4) has been successfully applied to complex systems in up to two dimensions [84].

A possible route to connect the geometry (local curvature) of a continuous surface to its topology (Euler characteristic) is given by the Gauss-Bonnet theorem [36]. In a simplicial complex, a discrete version of this theorem can be expressed as [48]

$$\chi = \sum_{i=1}^{N} \kappa_i(\varepsilon). \tag{5}$$

This connection has been explored in complex systems [84]. We also comment that the introduction of the node participation rank in Ref. [46] aimed to study the distribution of k-cliques in the human brain network, thus relating the appearance of cycles and cavities to the local network structure. Here, however, we intend to understand the topological phase transitions in brain networks from a local perspective, and to this end we compute the network curvature at each node, which also requires the knowledge of the node participation rank, as indicated by Eqs. (4) and (5).

In Fig. 7 we display results for the distribution of curvatures κ_i at the nodes (brain regions) of the functional brain network of the same individual depicted in Figs. 5 and 6. We choose three values of ε: one between the first and second topological transitions ($\varepsilon = 0.200$), one right at the second transition ($\varepsilon = 0.372 \approx \varepsilon_c$), and one after the second transition ($\varepsilon = 0.500$). [Note from the bottom panel of Fig. 4(b) that the threshold value at the second transition averaged over all individuals in the VUmc data set is slightly higher, $\varepsilon_c \approx 0.420$.] First, we remarkably verified the Gauss-Bonnet theorem, Eq. (5), for all ε's considered. This attests the self-consistency of our TDA approach as well as the robustness of the local-to-global connection in the context of brain networks.

Moreover, we further point that the local curvature of most nodes at the topological transition is null (a locally "flat" network), as also illustrated in the spatial brain representation in Fig. 7(b). Indeed, the mean local curvature is identically zero at the transition point $\varepsilon = 0.372 \approx \varepsilon_c$. This contrasts with the negative mean curvature (-0.39) before the transition at $\varepsilon = 0.200$ and positive mean curvature (0.20)

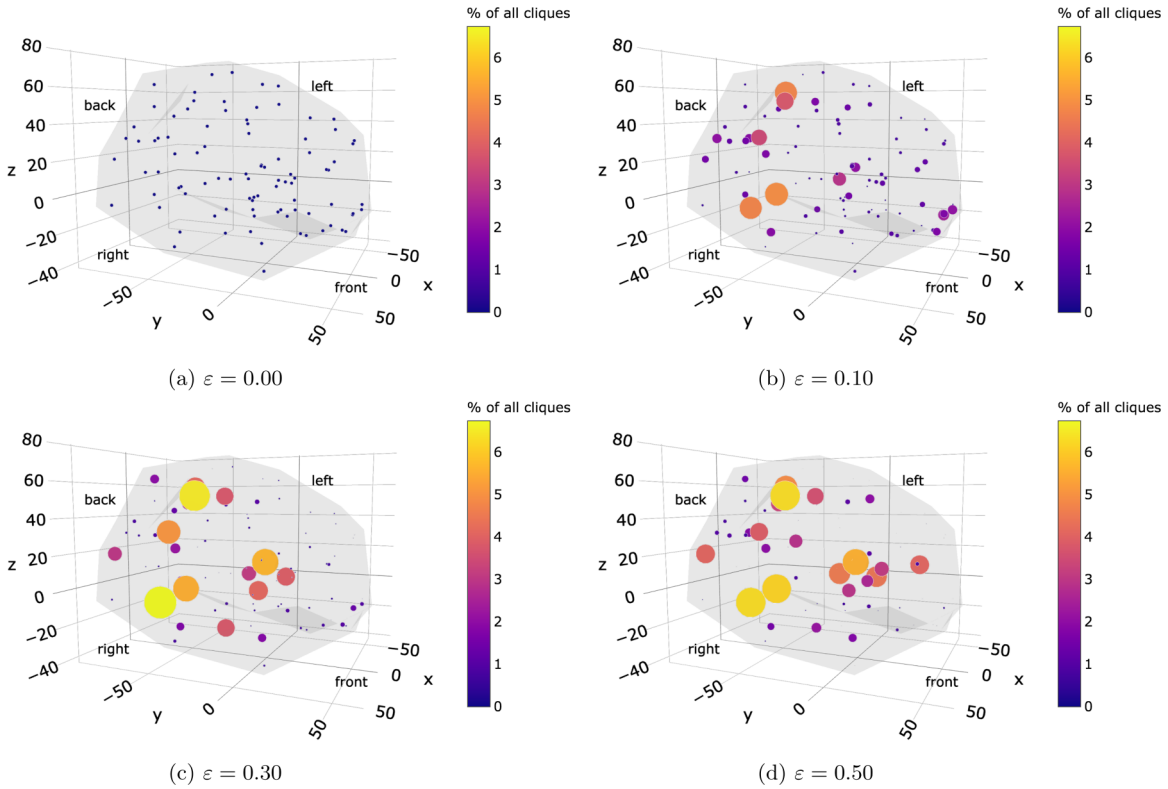

(a) $\varepsilon = 0.00$ (b) $\varepsilon = 0.10$

(c) $\varepsilon = 0.30$ (d) $\varepsilon = 0.50$

FIG. 6. Participation of brain regions in *all* connected (k-cliques) structures of a functional brain network. The most important brain regions (regarding the clique structure) are the ones with higher participation ranks. The distribution of participation ranks in all k-cliques allows us to compute the curvature of the brain network at each brain region, thus providing a local-to-global (geometry-topology) connection (see also Fig. 7). Moreover, the spatial analysis of participation ranks also opens the perspective of establishing a link between local network structure and brain function [46].

after the transition at $\varepsilon = 0.500$. Figure 7 also illustrates this picture in the form of a one-sheet hyperboloid surface of negative curvature at $\varepsilon < \varepsilon_c$, a locally flat cone of null curvature at $\varepsilon = \varepsilon_c$, and a two-sheet hyperboloid with positive curvature at $\varepsilon > \varepsilon_c$. Remarkably, from Eq. (5) a null mean curvature implies $\chi = 0$, which is also consistent with the assertion of the zeros of the Euler characteristic and singularities of the Euler entropy to set the location of the topological phase transitions in functional brain networks.

The local network structure defined both by the node participation rank in k-cliques and local curvature allows us to undoubtly differentiate functional brain networks from Erdős-Rényi random networks. Indeed, in Erdős-Rényi graphs those quantities are homogeneous over the nodes, which contrasts markedly with Figs. 5–7. Consequently, due to the same probability p of setting an edge linking any pair of nodes, in the case of a random network the colors and sizes of circles in Figs. 5–7 would appear essentially undifferentiated.

Finally, we also comment that the above scenario resembles significantly the behavior of some physical systems in the vicinity of phase transitions, at which the curvature of the equipotential energy surface in the configuration space is asymptotically null [26,85]. Indeed, an analogous evolution of the conic and hyperboloid surfaces shown in Fig. 7 can be also found for the equipotencial surface of some magnetic spin systems [26]. In this context, it is important to remark on a very recent empirical description [86] of the Betti numbers associated with different smells that can be described theoretically using a three-dimensional hyperbolic space, which has negative curvature. In fact, the relation between Betti numbers and curvature is well known for surfaces [87], and thus a possible extension of such relation for a simplicial complex can be possibly done.

In this work, we use the curvature as some sort of local version of the Euler characteristic in the context of the Gauss-Bonnet theorem proposed by Knill [47]. However, it is important to notice that there are other alternative definitions of curvature that could be observed in a complex network as well [88]. As examples we mention the Forman-Ricci curvature [89] and the Ollivier-Ricci curvature [90], which have been extensively applied to complex networks [91–94]. In particular, the Forman-Ricci curvature was studied in brain networks in Ref. [95]. In principle, one approach using a curvature metric that fulfills the Gauss-Bonnet theorem would lead to results analogous to the ones reported in that work concerning the relation between the curvature of a network and its Euler characteristic. For the Forman-Ricci curvature, there is indeed a recent version of the Gauss-Bonnet theorem [96]. Therefore, from the theoretical point of view we believe that analogous results could be obtained via the Forman-Ricci curvature. However, in contrast to the curvature proposed by Knill [47], there is a practical limitation to implement the Forman-Ricci curvature in order to observe a high-dimensional version of the Gauss-Bonnet theorem [96]. Thus, at the present we

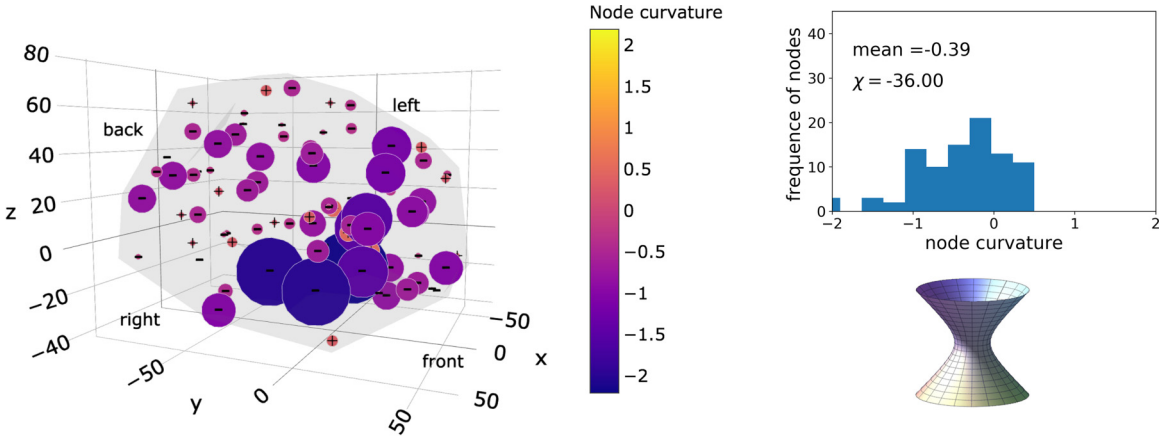

(a) $\varepsilon = 0.2 < \varepsilon_c$.

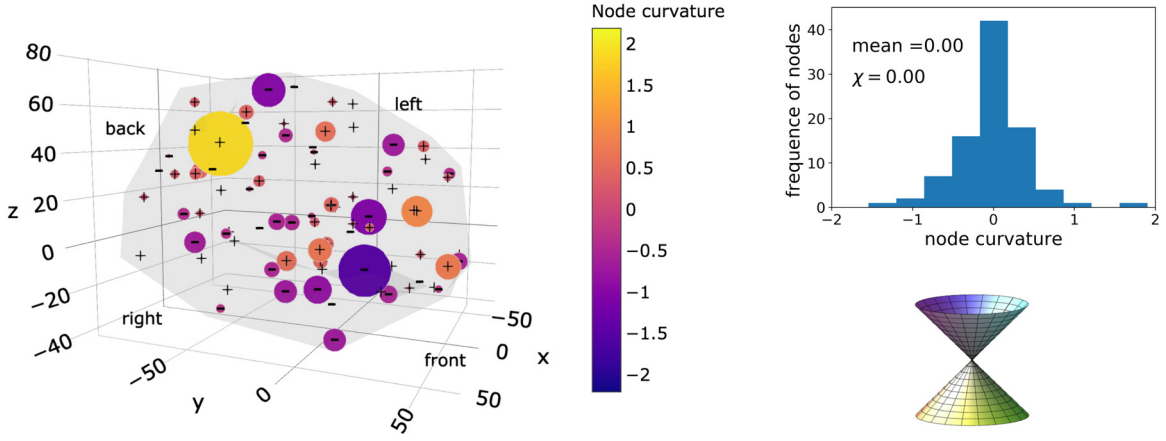

(b) $\varepsilon = \varepsilon_c = 0.372$.

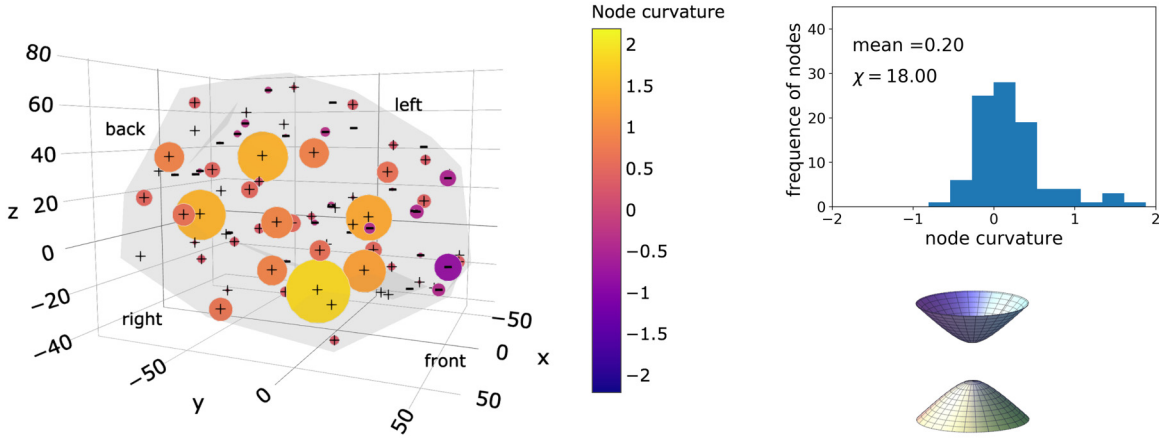

(c) $\varepsilon = 0.5 > \varepsilon_c$.

FIG. 7. Local-to-global connection in a functional brain network. (a) A one-sheet hyperboloid (top surface) has negative curvature. (b) By tightening the neck of the hyperboloid, it is deformed into a cone (mid surface), which has zero curvature. (c) By detaching the pieces of the cone and smoothing it, one finds a two-sheet hyperboloid (bottom surface), which has positive curvature. A similar evolution occurs for the curvature of the nodes in a functional brain network as a function of the threshold ε. The left brain plots illustrate the spatial location of sites of negative, null, and positive curvatures, whose distribution is displayed in the histograms. At the topological phase transition ($\varepsilon = \varepsilon_c$) of the brain network the mean curvature is null (midpanel). This point separates brain networks with negative ($\varepsilon < \varepsilon_c$) (top panel) and positive ($\varepsilon > \varepsilon_c$) (bottom panel) mean curvatures, just as the cone separates the one-sheet and two-sheet hyperboloids, precisely at the zeros of the Euler characteristic and singularities of the Euler entropy.

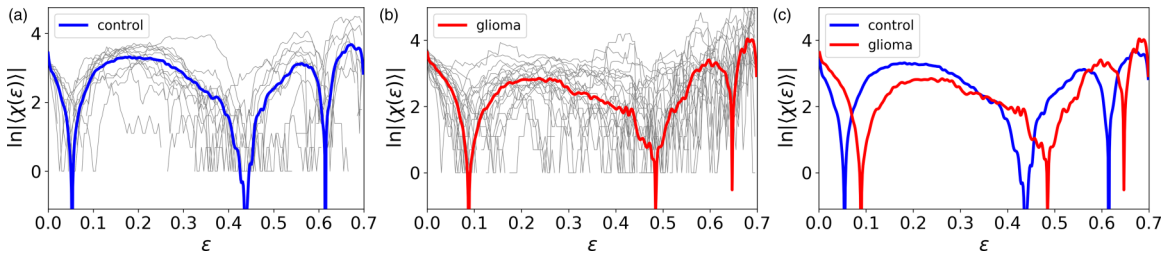

FIG. 8. Topological phase transitions in functional brain networks built from data sets constituted of (a) healthy individuals and (b) glioma patients with data taken from Ref. [32]. Individuals' results for the Euler entropy are shown in thin gray lines, whereas their average are depicted in thick colored lines. We compare directly both groups in (c), in which it is notice that, on average, the Euler entropy associated with the glioma group is shifted to the right, in comparison with the results from the control group. This finding gives paradigmatic evidence for the use of the critical points of topological phase transitions in functional brain networks as topological biomarkers.

cannot test whether the Forman-Ricci curvature also captures the topological phase transitions observed here. All these findings reinforce the connection between topology, geometry, and physics to evidence and characterize the topological phase transitions in functional brain networks.

D. Paradigmatic evidence of topological phase transitions as topological biomarkers

In the previous sections, we have described methods to generally detect and characterize topological phase transitions and applied them to both Erdős-Rényi random networks and functional brain networks. It is important to notice that the critical value of the control parameter at which the phase transition takes place is usually a system's fingerprint [53], as mentioned in the *Introduction*. Thus, one question that naturally emerges in this context is whether topological phase transitions in functional brain networks can be used as topological biomarkers, i.e., whether the critical points of the topological phase transitions could be applied to characterize different groups of brain networks.

We now compare the topological phase transitions in functional brain networks built from the healthy controls in the VUmc data set (control group) with those of an additional set of 21 individuals newly diagnosed with glioma (glioma group), recently reported in Ref. [32]. Glioma is the most frequently occurring primary brain tumor, which is associated with poor prognosis and oftentimes burdensome symptoms, like epileptic seizures and cognitive deficits. Importantly, these two groups were matched regarding age and sex, while the rs-fMRI data were obtained with identical scanning protocols. The functional brain networks built from both groups have been already reported in the literature using standard network metrics, which showed *no* difference in particular (hub) connectivity patterns currently thought to represent pathological network organization, although patients did have a globally distinct connectivity frequency distribution from the controls [32].

We applied our analysis to both groups of individuals, emphasizing that the computation of the Euler characteristic directly from the k-cliques of the network is more efficient than that using Betti numbers [15], which allowed us to reach correlation threshold levels up to $\varepsilon = 0.7$. This range of ε was actually sufficient to identify three topological phase transitions, as illustrated for the control group in Fig. 8(a) and for the glioma group in Fig. 8(b). We clearly see, by comparing the results of both groups superposed in Fig. 8(c), that, on average, the critical points of the topological phase transitions are shifted to the right in the glioma group. Therefore, we can interpret this shift as a possible reorganization of correlation patterns in the functional brain networks of the glioma group. Consequently, our results provide paradigmatic evidence for the use of topological phase transitions as a topological biomarker of dysfunctioning in functional brain networks.

It is important to observe, however, that the anatomic location, overall survival, and subtypes of glioma are usually quite different among patients [97]. For this reason, despite the fact that our results may represent a compelling advance in clinical network neuroscience, they only suffice to characterize average differences between control and glioma patients at a group level at this stage. Moreover, the glioma variability can be consistently associated with the larger fluctuations in the peaks of the Euler entropy illustrated in Fig. 8(b), when compared with the control group results in Fig. 8(a).

We also remark that a topological phase transition can be generally seen as an intrinsic property of the complex network, even though the actual position of the transition may depend on the way the filtration scheme is implemented. That was indeed the case for the functional brain networks analyzed in this work, in which the filtration was based on the absolute value of the correlations between areas of the brain in the HCP data set, while for the VUmc data set it was applied from the z-scores of correlations.

Another possibility is to base the filtration on the density of networks, which we prove in the following to be also of relevance for the interpretation of our results on the glioma networks. In fact, one could argue that, since the links corresponding to the lesions should be removed for a proper network analysis in the glioma group [32], then the results illustrated in Fig. 8 can be due to a change in the density of the glioma networks when compared to the healthy controls. In order to verify this possibility, we further performed a density-based filtration in the same data sets. In practice, we attached the most correlated areas in the brain networks so that all networks must have the same density $\rho \in [0, 1]$ at each step of the filtration scheme. In Fig. 9, we illustrate the Euler characteristic as a function of the density threshold for both control and glioma groups. Just as observed in Fig. 8, we can also distinguish between both groups through this

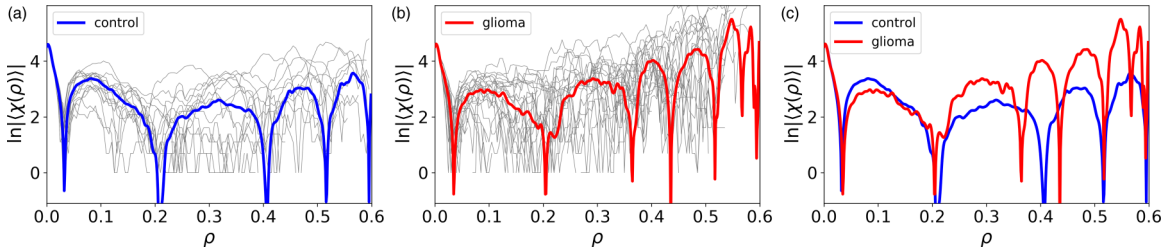

FIG. 9. Topological phase transitions in functional brain networks built from data sets constituted of (a) healthy individuals and (b) glioma patients as in Fig. 8 but now using a filtration scheme based on the density of networks. In contrast with Fig. 8, in which the filtration was based on the correlation threshold of brain correlations, differences between the two groups appear only for density values not too small, particularly in higher-order transitions. This result is compatible with the analysis in Ref. [32], since in the low-density range networks are mainly constituted of edges and triangles.

process. However, in contrast to the filtration based on the correlation threshold of correlations, the difference between the two groups emerges only for the topological phase transitions of higher orders, i.e., beyond the second peak. For lower densities, the functional brain networks are mainly constituted of edges, links, and triangles, and therefore our results in this low-density range are actually compatible with those of Ref. [32], with no group difference detected under standard network metrics, which in fact are usually based on low-dimensional structures (edges, paths, and triangles).

Some significant issues should be addressed in the future to better understand the potential use of topological invariants as biomarkers in functional brain networks. In this regard, although in a previous work [32] no difference was found in the traditional analysis of network topology between glioma patients and controls, there was a distinction found in the connectivity frequency distribution regarding these groups. Therefore, the relationship between the connectivity frequency distribution and topological phase transitions remains an open question that deserves subsequent investigation. Moreover, from a neuroscience perspective, a detailed assessment of the patients' characteristics and further comparison with TDA metrics should also be made in the future. For instance, one issue is whether the fact that not considering the regions with a tumor in the brain network could affect the topological phase transitions in the glioma group. This point has been already addressed when studying standard network metrics [32], but it is actually unknown from a TDA perspective. In short, further studies using the present methodology are necessary in order to better characterize the reorganization of the brain network in an individual level, taking into account the complexity and variety of glioma [97].

III. DISCUSSION AND CONCLUSIONS

The discovery that topological phase transitions occur in functional brain networks brings in its wake a number of striking consequences.

The universality principle of phase transitions states that a few properties of the system suffice to determine its macroscopic behavior close to the transition [53,54]. In this sense, systems that share those properties, but are microscopically distinct, display the same behavior near the phase transition. Conversely, the critical value of the control parameter at which the phase transition takes place is a system's fingerprint that can be used to differentiate it from others. Here we have located and characterized a sequence of topological phase transitions, associated with important changes in the topology of functional brain networks, by employing the TDA approach along with tools and concepts from topology and differential geometry and their relation to theoretical physics.

From the framework point of view, our results give strong support for the use of the Euler characteristic and entropy, Betti numbers, node participation in k-cliques structures, and distribution of local curvature as topological and geometrical markers closely associated with functional brain networks in particular and data-driven complex networks with embedded correlations in general. In this sense, our work, together with other recent initiatives that also applied topology ideas to neuroscience [45,46,49,52,59,60,98,99], reinforces the conjecture made by Zeeman in 1965 that topology is a natural mathematical framework to capture the underlying global properties of the brain [100].

The connection between the local (geometrical) and global (topological) structures in brain networks has been firmly evidenced in our results. The topological phase transitions are equally determined both from topological quantities (zeros of Euler characteristic and singularities of Euler entropy), as well as from local geometrical measurements, through the null mean curvature at nodes (brain regions) of the functional brain network. From these quantities, we also found a remarkable confirmation of the discrete Gauss-Bonnet theorem in brain networks.

The geometrical interpretation of the topological phase transitions observed in brain networks is analogous to the generalization of the percolation transition for higher-dimensional structures [13,23,34]. This leads to an interesting insight related to the critical brain hypothesis, which states that the brain is a high-dimensional dynamical system operating in the vicinity of a phase transition [56,101–104]. In fact, in Refs. [105,106] the authors consistently argue that the fundamental features of the spontaneous resting state brain activity exists, regardless of any filtration parameter, nearby the giant-component transition, which corresponds to the first topological phase transition observed in our work.

The potential implications of the present approach are overarching. On the one hand, the fact that our TDA analysis is multidimensional consequently yields an ampler range of available information on the brain's intrinsic structure and connections, without necessarily increasing the number

of (subjectively chosen) working parameters. Moreover, the identification of reliable biomarkers of individual and group differences is a crucial issue in clinical neuroscience and personalized medicine. In this context, the location of the topological phase transitions in functional brain networks have potential to be used as a topological biomarker. The TDA framework allows us to classify the location sequence of topological transitions in brain networks both at the individual and collective levels, thus enabling direct comparisons with control group standards. A change in the location pattern of the topological transitions may signal an important change in the correlations among brain regions. It can therefore be fundamentally related to possible suboptimal brain functioning [55–57] and may become a relevant precision tool in the clinical diagnosis of neurological and psychiatric disorders [58]. In fact, here we have provided some evidence for such applications by comparing topological phase transitions between healthy controls and glioma patients. Further studies on this issue will be left for a future work.

We have also shown that our approach is able to spatially locate the brain regions that participate most in the connected structures of the functional brain network. This finding may give rise to potential advances in the quest for a proper link between the local network structure and brain function.

We also remark that the joint use of the TDA approach with concepts from topology, geometry, and physics is certainly not restricted to the study of brain networks. Actually, this interdisciplinary framework can be readily applied to look into topological and geometrical properties of other complex networks, such as proteomic, metabolomic, and gene expression, to name a few. These ideas, together with further theoretical insights from TDA, may allow a qualitative change in the big data analysis, moving from theory-blind machine learning to a firmer ground based on an intrinsic way of connecting empirical data to the theoretical formalism of these disciplines.

Last, our work is also possibly related to one of the most important current scientific debates: Does one miss causality when studying complex phenomena from the big data perspective? Most large data sets generated nowadays under the big data approach are concerned with analyses and predictions based on statistical correlations only, therefore usually lacking causality relations established from a solid theoretical background [107]. In this sense, putting together ideas from those well-grounded theoretical fields to treat big data-driven complex systems may appear as a promising way to settle this question [28]. Just like this multiple-field analogy proved to be fruitful here, there are many other results connecting topology, geometry, and theoretical physics (see *Methods*) that may help one to navigate and improve the vast repertoire of tools available in TDA. In the same way that Riemannian geometry enabled the development of general relativity, the emerging field of TDA has potential to trigger principles that could boost the understanding of the big data revolution from this interdisciplinary perspective.

In conclusion, the discovery of topological phase transitions in brain networks can open the perspective for establishing reliable topological and geometrical biomarkers of individual and group differences. The joint use of interdisciplinary concepts and tools under the TDA approach might change the way complex systems data are analyzed, and can contribute to solve currently open significant questions related to complex networks in various fields, including neuroscience and medicine.

IV. METHODS

A. Theoretical support from the connection among topology, geometry, and physics

The impact of the use of tools and ideas from topology and differential geometry has permeated many areas of science. In fact, by applying Riemannian differential geometry, Einstein in his theory of gravity (general relativity) has changed our conception of the space-time structure in the presence of massive cosmological objects [108]. It still thrives and has led to surprising theoretical findings and recent groundbreaking experimental discoveries, including black holes and gravitational waves [109].

On the other hand, topology has played a seminal role in several areas of modern physics. Indeed, topological quantum field theory is now a mature topic [44,110], while the description of several phenomena in condensed matter physics has achieved a deeper understanding by taking advantage of topological concepts [2,3]. The bridge between topology and differential geometry can be established through theorems that link local properties of a system with global ones, such as the Gauss-Bonnet theorem [36].

One of the greatest achievements of the use of topology ideas in physics concerns the introduction of the concept of topological phase transition [2,3]. Examples range from the integer and fractional quantum Hall effects to topological insulators, including the quest for quantum computation [2,3,111,112]. As a consequence, the notion of the topological phase of matter has emerged. Its distinction from the usual phases of matter that undergo equilibrium phase transitions has been emphasized, notably the absence of symmetry breaking or a local order parameter, as well as the role played by topological invariants that provide stability (protection) against perturbations [2,3,111,112]. Also, the identification of topological phases, either in quantum or classical physical systems, has recently received special attention in the context of machine-learning ideas [113].

In addition, much effort has been also devoted to characterize phase transitions in the configuration space of a physical system from a topological viewpoint [7,8]. For instance, the concepts of Euler characteristic and Euler entropy have been introduced in a number of exactly solvable models [7,10,24–26] whose energy is described by a Hamiltonian function. Remarkably, in those systems the singularities of the Euler entropy were found to take place precisely at the phase transitions. This result resembles the statement of the Yang-Lee theorem [73], according to which the singular behavior exhibited by thermodynamic quantities in equilibrium phase transitions coincide precisely with the zeros of the system's partition function.

The picture gains in complexity when it turns to the case of topological phase transitions occurring in complex networks. In this context, the system's Hamiltonian is usually missing (or nonexistent), and instead of studying the system behavior

as a function of energy, intrinsic correlations between the system constituents determined from empirical data define the network topology. Therefore, the Euler characteristic and entropy, as well as the Betti numbers (see main text), emerge in this scenario as natural quantities to look into topological phase transitions in complex networks, particularly in the functional brain networks investigated here.

A number of computational topology tools has been successfully applied to the multidimensional analysis of complex networks [6]. For instance, persistent homology [16] has been employed across fields, such as contagion maps [114] and materials science [115]. Moreover, a direct evidence of topological differences in classical phase transitions of the XY mean-field model and the ϕ^4 lattice model was found using methods of persistent homology [116]. In neuroscience, it has also yielded quite impactful results [45,46,52,98,117–119]. In this context, the Blue Brain Project recently provided persuasive support based both on empirical data and theoretical insights for the hypothesis that the brain network comprises topological structures in up to 11 dimensions [49].

At this point one final remark is in order. Why is the above discussion about the interdisciplinary relations among topology, geometry, physics, neuroscience, and big data research important? The results of the present work entail that, to a certain extent, correlations in functional brain networks are driven by principles that find some equivalence in the connections among phase transitions in physics, topology, and differential geometry. In this sense, one may argue that such relations might not be exclusive to functional brain networks but instead can be part of a much wider picture featuring general data-driven complex systems that usually lack a Hamiltonian formulation. If so, then the present study can shed light on a possible theoretical route based on such connections to explain the huge success of modeling similarity data using artificial intelligence and machine-learning techniques.

B. TDA approach and brain correlation matrices

Here we provide further technical details on the TDA approach applied to Erdős-Rényi random networks and functional brain networks.

In the case of brain networks, we analyzed extensively two data sets (HCP and VUmc, see below) containing information on the correlations among brain regions in the form of raw data and z-score data, respectively. These distinct forms were purposefully chosen to represent the diversity of approaches in the literature for measures of similarity among brain regions in brain networks [18].

We start with the analysis of the rs-fMRI measurements from the HCP data set [120] under the 1000 Functional Connectomes Project [121]. It comprises data from 986 individuals, with the brain subdivided into $N = 177$ regions. The rs-fMRI measurements generate one time series for the activity of each particular brain region of each individual. It is thus possible to calculate the raw correlation between each pair of brain regions i and j of each individual by means of a Pearson correlation coefficient $C_{ij} \in [-1, 1]$, with $i, j = 1, \ldots, N$. Therefore, in this case one is left with an $N \times N$ matrix C_{ij} of raw correlations among brain regions for each individual.

Once the correlation matrices C_{ij} are built, the next step is the filtration process. In a physical system, where the energy is described by a Hamitonian function, the study of the topology of the configuration space can be done by sweeping up the energy levels in the equipotential energy surface [7,10,24–26] (see Fig. 1). Here, instead of the energy of a physical system or the variable that controls the height function in Morse theory, we define a filtration parameter in the form of a correlation threshold level ε as follows.

It is usually considered [122] that a small, nonzero value of C_{ij} may just reflect noise rather than the existence of any actual functional connection between brain regions i and j. To circumvent this problem, a thresholding is typically applied [18] in order to retain only correlations whose absolute value $|C_{ij}|$ lies above some given correlation threshold level $\varepsilon \in [0, 1]$. In mathematical terms, we write

$$|C_{ij}| \to |C_{ij}|(\varepsilon) = \begin{cases} 0, & \text{if } |C_{ij}| \leqslant 1 - \varepsilon \\ |C_{ij}|, & \text{otherwise} \end{cases}. \tag{6}$$

Conventionally, the diagonal elements $|C_{ii}|$ are set up to zero [122]. A functional brain network can thus be constructed from the matrix $|C_{ij}|(\varepsilon)$ in Eq. (6) by assigning an edge connecting the brain regions i and j if $|C_{ij}| \neq 0$ at the given value ε. In this sense, Eq. (6) defines a connectivity matrix [18] of the functional brain network for each ε. For example, a network with no links corresponds to $\varepsilon = 0$, whereas a fully connected structure arises for $\varepsilon = 1$. Furthermore, since the edges are generally associated with values $0 < |C_{ij}| \leqslant 1$, then the matrix also relates to the normalized weighted adjacency matrix in graph theory [18], whose elements represent the connection weights between each pair of nodes in the network.

Although thresholding is a widely used technique in functional brain networks, it is in fact not yet clear what is the best strategy to choose the proper threshold value [18]. At this point, an analogy with Morse theory can be useful since one could track the topological evolution of the brain network as a function of ε in a way similar to level sets in a process called filtration [16,22,118], as explained below.

A graph with nodes and linking edges can represent a network structure. The filtration of a complex network is obtained by thresholding its connectome matrix for values $\varepsilon \in [0, 1]$ and subsequently ordering the resulting evolving graphs for increasing ε: $\emptyset \subset G_{\varepsilon_1} \subset \ldots G_{\varepsilon_i} \subset G_{\varepsilon_{i+1}} \ldots \subset G_1$, with the totally unconnected (empty) graph $\emptyset = G_0$, fully connected (complete) graph G_1, and $\varepsilon_i < \varepsilon_{i+1}$ (see Fig. 1). Here we implemented a filtration process using the Python NetworkX library [123].

The bridge between TDA, network theory, and the topological approach to phase transitions is built through the calculation of topological quantities [22] such as the Euler characteristic and entropy and the set of Betti numbers as a function of ε. To this aim, it is necessary to compute the numbers of k-cliques in a graph, i.e., subgraphs with k all-to-all connected nodes (see Sec. II). The computational effort to find a k-clique in a complex network is an NP-complete problem [124]. It means that, as more edges are attached, the numerical difficulty increases exponentially. For this reason,

in the functional brain networks analyzed here we calculated the Euler characteristic using the NetworkX package up to the maximum threshold level $\varepsilon = 0.60$. Moreover, we further observed that the convergence times to finish the computation of the k-cliques distribution are distinct for each individual brain network. Thus, as some networks presented prohibitively long convergence, we also applied a maximum cutoff processing time. Under this procedure, the brain networks of 420 individuals could reach the maximum threshold $\varepsilon = 0.60$, see Figs. 3 and 4.

An even greater difficulty appeared in the calculation of the Betti numbers β_n (see Sec. II A). In this case, in order to circumvent the long processing times we employed the concept of masked arrays [125], which performs averages of Betti numbers according to the number of brain networks that reached a given threshold level. Since the convergence time becomes increasingly longer for higher ε's, not all networks reached the maximum value $\varepsilon = 0.50$ displayed in Fig. 4, which explains the higher fluctuations in β_n near this threshold level. We managed to compute, for a maximum period of 30 days of computing time, 712 individuals networks up to $\varepsilon = 0.50$, which is above the first two topological phase transitions analyzed in detail.

We now turn to the VUmc data set [32], in which rs-fMRI measurements were performed using a different scanner and under different preprocessing steps in 15 healthy controls and 21 glioma patients, with the brain subdivided into $N = 92$ regions. Both groups were matched with regard to age and sex and underwent identical scanning and data processing. In the glioma group, regions containing tumor were masked out of the rs-fMRI in order to exclude artifactual time series. Most numerical procedures applied to the VUmc data set were quite similar to the ones of the HCP datset. Nevertheless, instead of raw correlation data, a different approach in terms of z-score values of correlations was employed in the VUmc data set. Indeed, the matrix elements C_{ij} were obtained as in the HCP data set, in the form of a Pearson correlation coefficient. However, after taking their absolute value we computed the z-score values of correlations for each matrix element, i.e., the number of standard deviations by which the correlation value differs from the average, and proceeded the subsequent TDA study as in the case of the HCP data set. This procedure ensures that slight differences in the overall connectivity strength induced by scanner differences or other nonphysiological parameters are disregarded in the analysis.

Last, we also mention that a similar study was performed in the Erdős-Rényi random networks, with the probability p of linking two nodes playing the role of the correlation threshold level ε in the filtration process (see Sec. II A). In this case, however, we did not face the difficulty related to long processing times to compute the numbers of k-cliques since an exact analytical expression [48] is available for Erdős-Rényi graphs, Eq. (1). Thus, we were able to sweep the whole interval $p \in [0, 1]$ in the calculation of the Euler characteristic and entropy of Erdős-Rényi networks, as shown in Fig. 2. Nevertheless, regarding the computation of the Betti numbers in Fig. 2, since an analytic expression for β_n is not at hand, in this case we actually performed numerical simulations of smaller Erdős-Rényi networks ($N = 25$ nodes) and linking probabilities in the range $p \in [0, 0.7]$.

ACKNOWLEDGMENTS

F.A.N.S., E.P.R., M.D.C.F., and M.C. acknowledge the financial support from CAPES, CNPq, and FACEPE through the PRONEX Program (APQ-0602-1.05/14) (Brazilian agencies). M.C. is funded by the FAPESP Center for Neuromathematics (2013/07699-0) and through FACEPE/FAPESP program (APQ–0642–1.05/18). L.D. is funded by an NWO Veni (016.146.086) and a Branco Weiss Fellowship. Data were provided by the Human Connectome Project, WU-Minn Consortium (Grant No. 1U54MH091657), funded by the 16 NIH Institutes and Centers that support the NIH Blueprint for Neuroscience Research, and by the McDonnell Center for Systems Neuroscience at Washington University. F.A.N.S. and L.D. would like to thank the NWO visitor's travel grant (040.11.693). Data processed at VUmc were kindly provided by Dr. M. Raemaekers, from the Department of Neurology and Neurosurgery, Brain Center Rudolf Magnus, University Medical Center Utrecht. F.A.N.S. would also like to thank fruitful discussions with Sostenes Lins, Heather Harrington, Ulrike Tillmann, Fernando Moraes, Eamonn A. Gaffney, Jeffrey Giansiracusa, Pawel Dlotko, Marco Baroni, Cleide Martins, Renê R. Montenegro-Filho, Bertrand Berche, Victor Caldas, Dante Chialvo, Stephan Boettcher, Tom Shimizu, and James P. Crutchfield during the development of this work.

F.A.N.S. developed the theoretical formalism and performed the calculations and numerical simulations of the Erdős-Rényi random networks and functional brain networks. L.D. and F.A.N.S. proposed the search for topological phase transitions in brain networks. E.P.R. and M.D.C.F. proceeded the scaling analysis and fitting of the data near the phase transition point. F.A.N.S. and E.P.R. wrote the first version of the manuscript. All authors were involved in the subsequent writing and development of the manuscript. All authors planned the research and discussed the results.

[1] M. Gromov, *Local and Global in Geometry* (IHES, Bures-sur-Ivette, France, 1999).
[2] F. D. M. Haldane, Rev. Mod. Phys. **89**, 040502 (2017).
[3] J. M. Kosterlitz, Rev. Mod. Phys. **89**, 040501 (2017).
[4] R. Daw, Nature **493**, 168 (2013).
[5] R. Thom, Topology **8**, 313 (1969).
[6] G. Petri, M. Scolamiero, I. Donato, and F. Vaccarino, PLoS ONE **8**, e66506 (2013).
[7] M. Pettini, *Geometry and Topology in Hamiltonian Dynamics and Statistical Mechanics*, Interdisciplinary Applied Mathematics, Vol. 33 (Springer, New York, 2007).
[8] M. Kastner, Rev. Mod. Phys. **80**, 167 (2008).
[9] M. Buchanan, Nat. Phys. **4**, 5 (2008).

[10] F. A. N. Santos, L. C. B. d. Silva, and M. D. Coutinho-Filho, J. Stat. Mech.: Theory Exp. (2017) 013202.

[11] M. Gori, R. Franzosi, and M. Pettini, J. Stat. Mech.: Theory Exp. (2018) 093204.

[12] D. Gandolfo, Physica A **358**, 22 (2005).

[13] E. Roubin and J.-B. Colliat, J. Stat. Mech.: Theory Exp. (2016) 033306.

[14] G. Carlsson, Bull. Am. Math. Soc. **46**, 255 (2009).

[15] H. Edelsbrunner and J. Harer, *Computational Topology: An Introduction* (American Mathematical Society, Providence, RI, 2010), p. 241.

[16] N. Otter, M. A. Porter, U. Tillmann, P. Grindrod, and H. A. Harrington, EPJ Data Science **6**, 17 (2017).

[17] A.-L. Barabasi and M. Posfai, *Network Science* (Cambridge University Press, Cambridge, UK, 2016).

[18] A. Fornito, A. Zalesky, and E. T. Bullmore, *Fundamentals of Brain Network Analysis* (Academic Press, London, 2016).

[19] M. Kahle, AMS Contemp. Math. **620**, 201 (2014).

[20] V. Salnikov, D. Cassese, and R. Lambiotte, Eur. J. Phys. **40**, 014001 (2018).

[21] Y. Holovatch, R. Kenna, and S. Thurner, Eur. J. Phys. **38**, 023002 (2017).

[22] R. W. Ghrist, *Elementary Applied Topology* (CreateSpace, Scotts Valley, CA, 2016).

[23] N. Linial and Y. Peled, Ann. Math. **184**, 745 (2016).

[24] L. Angelani, L. Casetti, M. Pettini, G. Ruocco, and F. Zamponi, Europhys. Lett. **62**, 775 (2003).

[25] L. Casetti, M. Pettini, and E. G. D. Cohen, J. Stat. Phys. **111**, 1091 (2003).

[26] F. A. N. Santos and M. D. Coutinho-Filho, Phys. Rev. E **80**, 031123 (2009).

[27] Y. Matsumoto, *An Introduction to Morse Theory* (American Mathematical Society, Providence, RI, 2002).

[28] W. Bialek, Rep. Prog. Phys. **81**, 012601 (2018).

[29] B. Bollobas, *Random Graphs* (Cambridge University Press, Cambridge, UK, 2001).

[30] D. C. Van Essen, K. Ugurbil, E. Auerbach, D. Barch, T. E. J. Behrens, R. Bucholz, A. Chang, L. Chen, M. Corbetta, S. W. Curtiss, S. Della Penna, D. Feinberg, M. F. Glasser, N. Harel, A. C. Heath, L. Larson-Prior, D. Marcus, G. Michalareas, S. Moeller, R. Oostenveld, S. E. Petersen, F. Prior, B. L. Schlaggar, S. M. Smith, A. Z. Snyder, J. Xu, and E. Yacoub, NeuroImage **62**, 2222 (2012).

[31] D. S. Marcus, J. Harwell, T. Olsen, M. Hodge, M. F. Glasser, F. Prior, M. Jenkinson, T. Laumann, S. W. Curtiss, and D. C. Van Essen, Front. Neuroinf. **5**, 4 (2011).

[32] J. Derks, A. R. Dirkson, P. C. de Witt Hamer, Q. van Geest, H. E. Hulst, F. Barkhof, P. J. W. Pouwels, J. J. G. Geurts, J. C. Reijneveld, and L. Douw, NeuroImage: Clinical **14**, 87 (2017).

[33] O. Knill, On the dimension and Euler characteristic of random graphs, arXiv:1112.5749 (2011).

[34] M. Kahle, Discr. Math. **309**, 1658 (2009).

[35] J. H. Conway, H. Burgiel, and C. Goodman-Strauss, *The Symmetries of Things* (CRC Press, Boca Raton, FL, 2008), p. 426.

[36] M. P. Do Carmo, *Differential Geometry of Curves and Surfaces* (Dover, New York, 2016).

[37] J. F. Nash, Jr. and L. Nirenberg, The 2015 Abel Prize Lectures (2015), https://www.abelprize.no/c63466/binfil/download.php?tid=63579.

[38] R. A. Kycia, S. Kubis, and W. Wójcik, Phys. Rev. C **96**, 025803 (2017).

[39] R. Franzosi and M. Pettini, Phys. Rev. Lett. **92**, 060601 (2004).

[40] R. Franzosi and M. Pettini, Nucl. Phys. B **782**, 219 (2007).

[41] R. Franzosi, M. Pettini, and L. Spinelli, Nucl. Phys. B **782**, 189 (2007).

[42] O. Y. Viro, Some integral calculus based on euler characteristic, in *Topology and Geometry, Rohlin Seminar*, edited by O. Y. Viro (Springer, Berlin, 1988), p. 127.

[43] E. Witten, Nucl. Phys. B **202**, 253 (1982).

[44] E. Witten, J. Diff. Geom. **17**, 661 (1982).

[45] C. Giusti, E. Pastalkova, C. Curto, and V. Itskov, Proc. Natl. Acad. Sci. USA **112**, 13455 (2015).

[46] A. E. Sizemore, C. Giusti, A. Kahn, J. M. Vettel, R. F. Betzel, and D. S. Bassett, J. Comput. Neurosci. **44**, 115 (2018).

[47] O. Knill, A discrete Gauss-Bonnet type theorem, arXiv:1009.2292 (2010).

[48] O. Knill, On index expectation and curvature for networks, arXiv:1202.4514 (2012).

[49] M. W. Reimann, M. Nolte, M. Scolamiero, K. Turner, R. Perin, G. Chindemi, P. Dłotko, R. Levi, K. Hess, and H. Markram, Front. Comput. Neurosci. **11**, 48 (2017).

[50] H. Aerts, W. Fias, K. Caeyenberghs, and D. Marinazzo, Brain **139**, 3063 (2016).

[51] H. Edelsbrunner, D. Letscher, and A. Zomorodian, Discr. Comput. Geom. **28**, 511 (2002).

[52] G. Petri, P. Expert, F. Turkheimer, R. Carhart-Harris, D. Nutt, P. J. Hellyer, and F. Vaccarino, J. R. Soc., Interface **11**, 20140873 (2014).

[53] H. E. Stanley, *Introduction to Phase Transitions and Critical Phenomena* (Oxford University Press, Oxford, UK, 1987).

[54] C. Domb, *The Critical Point: A Historical Introduction to the Modern Theory of Critical Phenomena* (Taylor & Francis, London, 1996).

[55] C. J. Stam, Clin. Neurophysiol. **116**, 2266 (2005).

[56] D. R. Chialvo, Nat. Phys. **6**, 744 (2010).

[57] D. Plenz and E. Niebur (eds.), *Criticality in Neural Systems* (Wiley-VCH Verlag, Weinheim, Germany, 2014).

[58] C. Meisel, A. Storch, S. Hallmeyer-Elgner, E. Bullmore, and T. Gross, PLoS Comput. Biol. **8**, e1002312 (2012).

[59] M. Saggar, O. Sporns, J. Gonzalez-Castillo, P. A. Bandettini, G. Carlsson, G. Glover, and A. L. Reiss, Nat. Commun. **9**, 1399 (2018).

[60] B. J. Stolz, T. Emerson, S. Nahkuri, M. A. Porter, and H. A. Harrington, Topological data analysis of task-based fMRI data from experiments on schizophrenia, arXiv:1809.08504 (2018).

[61] H. Lee, H. Kang, M. K. Chung, B.-N. Kim, and D. S. Lee, IEEE Trans. Med. Imag. **31**, 2267 (2012).

[62] M. H. Poincaré, J. Ec. Polytech. **2**, 1 (1895).

[63] P. Blanchard, C. Dobrovolny, D. Gandolfo, and J. Ruiz, J. Stat. Mech.: Theory Exp. (2006) P03011.

[64] J. A. Rehn, F. A. N. Santos, and M. D. Coutinho-Filho, Braz. J. Phys. **42**, 410 (2012).

[65] P. Blanchard, S. Fortunato, and D. Gandolfo, Nucl. Phys. B **644**, 495 (2002).

[66] P. Blanchard, D. Gandolfo, J. Ruiz, and S. Shlosman, Markov Process. Relat. Fields **9**, 523 (2003).

[67] L. Speidel, H. A. Harrington, S. J. Chapman, and M. A. Porter, Phys. Rev. E **98**, 012318 (2018).

[68] M. F. Sykes and J. W. Essam, J. Math. Phys. **5**, 1117 (1964).

[69] B. L. Okun, J. Stat. Phys. **59**, 523 (1990).
[70] K. R. Mecke and H. Wagner, J. Stat. Phys. **64**, 843 (1991).
[71] R. A. Neher, K. Mecke, and H. Wagner, J. Stat. Mech.: Theory Exp. (2008) P01011.
[72] G. Bianconi and R. M. Ziff, Phys. Rev. E **98**, 052308 (2018).
[73] C. N. Yang and T. D. Lee, Phys. Rev. **87**, 404 (1952).
[74] C. E. Shannon, Bell Syst. Tech. J. **27**, 379 (1948).
[75] W. Mayer, Ann. Math. **43**, 370 (1942).
[76] W. Mayer, Ann. Math. **43**, 594 (1942).
[77] O. Knill, On Helmholtz free energy for finite abstract simplicial complexes, arXiv:1703.06549 (2017).
[78] T. Mainiero, Homological tools for the quantum mechanic, arXiv:1901.02011 (2019).
[79] P. Baudot and D. Bennequin, Entropy **17**, 3253 (2015).
[80] H. Edelsbrunner, Z. Virk, and H. Wagner, Topological data analysis in information space, arXiv:1903.08510 (2019).
[81] P. L. Antonelli and C. Strobeck, Adv. Appl. Probab. **9**, 238 (1977).
[82] See Supplemental Material at http://link.aps.org/supplemental/10.1103/PhysRevE.100.032414 for a movie illustrating a topological phase transition in a brain network through a geometric perspective and interactive versions of all three-dimensional brain network images.
[83] F. Morone, K. Roth, B. Min, H. E. Stanley, and H. A. Makse, Proc. Natl. Acad. Sci. USA **114**, 3849 (2017).
[84] Z. Wu, G. Menichetti, C. Rahmede, and G. Bianconi, Sci. Rep. **5**, 10073 (2015).
[85] M. Kastner and O. Schnetz, Phys. Rev. Lett. **100**, 160601 (2008).
[86] Y. Zhou, B. H. Smith, and T. O. Sharpee, Sci. Adv. **4**, eaaq1458 (2018).
[87] K. Yano and S. Bochner, *Curvature and Betti Numbers* (Princeton University Press, Princeton, NJ, 1953).
[88] L. Najman and P. Romon (eds.), *Modern Approaches to Discrete Curvature*, Lecture Notes in Mathematics, Vol. 2184 (Springer, Cham, Switzerland, 2017).
[89] R. Forman, Discr. Comput. Geom. **29**, 323 (2003).
[90] Y. Ollivier, J. Funct. Anal. **256**, 810 (2009).
[91] C.-C. Ni, Y.-Y. Lin, J. Gao, X. D. Gu, and E. Saucan, Ricci curvature of the internet topology, in *Proceedings of the 2015 IEEE Conference on Computer Communications (INFOCOM'15)* (IEEE, Los Alamitos, CA, 2015), p. 2758.
[92] R. S. Sandhu, T. T. Georgiou, and A. R. Tannenbaum, Sci. Adv. **2**, e1501495 (2016).
[93] R. S. Sandhu, T. T. Georgiou, E. Reznik, L. Zhu, I. Kolesov, Y. Senbabaoglu, and A. Tannenbaum, Sci. Rep. **5**, 12323 (2015).
[94] R. P. Sreejith, K. Mohanraj, J. Jost, E. Saucan, and A. Samal, J. Stat. Mech.: Theory Exp. (2016) 063206.
[95] M. Weber, J. Stelzer, E. Saucan, A. Naitsat, G. Lohmann, and J. Jost, Curvature-based methods for brain network analysis, arXiv:1707.00180 (2017).
[96] M. Weber, E. Saucan, and J. Jost, J. Complex Netw. **6**, 706 (2017).
[97] S. Larjavaara, M. Riitta, T. Salminen, H. Haapasalo, J. Raitanen, J. Juha, and A. Auvinen, Neuro-Oncology **9**, 319 (2007).
[98] P. Masulli and A. E. P. Villa, SpringerPlus **5**, 388 (2016).
[99] M. Piangerelli, M. Rucco, L. Tesei, and E. Merelli, BMC Res. Not. **11**, 392 (2018).
[100] E. C. Zeeman, Topology of the brain, in *Mathematics and Computer Science in Biology and Medicine* (H.M. Stationery Office, London, UK, 1965), p. 240.
[101] D. R. Chialvo, Physica A **340**, 756 (2004).
[102] J. M. Beggs, Philos. Trans. R. Soc., A **366**, 329 (2007).
[103] J. M. Beggs and N. Timme, Front. Physiol. **3**, 163 (2012).
[104] A. J. Fontenele, N. A. P. de Vasconcelos, T. Feliciano, L. A. A. Aguiar, C. Soares-Cunha, B. Coimbra, L. Dalla Porta, S. Ribeiro, A. J. Rodrigues, N. Sousa, P. V. Carelli, and M. Copelli, Phys. Rev. Lett. **122**, 208101 (2019).
[105] A. Haimovici, E. Tagliazucchi, P. Balenzuela, and D. R. Chialvo, Phys. Rev. Lett. **110**, 178101 (2013).
[106] E. Tagliazucchi, P. Balenzuela, D. Fraiman, and D. R. Chialvo, Front. Physiol. **3**, 15 (2012).
[107] R. E. Baker, J.-M. Peña, J. Jayamohan, and A. Jérusalem, Biol. Lett. **14**, 20170660 (2018).
[108] A. Einstein, *Sitzungsberichte der Königlich Preußischen Akademie der Wissenschaften* (Prussian Academy of Sciences, Berlin, 1915), pp. 844–847.
[109] B. Abbott *et al.* (LIGO Scientific Collaboration and Virgo Collaboration), Phys. Rev. Lett. **116**, 061102 (2016).
[110] M. F. Atiyah, Publ. Math. l'IHÉS **68**, 175 (1988).
[111] A. Kitaev and J. Preskill, Phys. Rev. Lett. **96**, 110404 (2006).
[112] M. Levin and X.-G. Wen, Phys. Rev. Lett. **96**, 110405 (2006).
[113] J. Carrasquilla and R. G. Melko, Nat. Phys. **13**, 431 (2017).
[114] D. Taylor, F. Klimm, H. A. Harrington, M. Kramár, K. Mischaikow, M. A. Porter, and P. J. Mucha, Nat. Commun. **6**, 7723 (2015).
[115] Y. Lee, S. D. Barthel, P. Dłotko, S. M. Moosavi, K. Hess, and B. Smit, Nat. Commun. **8**, 15396 (2017).
[116] I. Donato, M. Gori, M. Pettini, G. Petri, S. De Nigris, R. Franzosi, and F. Vaccarino, Phys. Rev. E **93**, 052138 (2016).
[117] D. S. Bassett and O. Sporns, Nat. Neurosci. **20**, 353 (2017).
[118] C. Giusti, R. Ghrist, and D. S. Bassett, J. Comput. Neurosci. **41**, 1 (2016).
[119] C. Curto, Bull. Am. Math. Soc. **54**, 63 (2016).
[120] J. A. Brown, J. D. Rudie, A. Bandrowski, J. D. Van Horn, and S. Y. Bookheimer, Front. Neuroinf. **6**, 28 (2012).
[121] D. Tomasi and N. D. Volkow, Proc. Natl. Acad. Sci. USA **107**, 9885 (2010).
[122] K. Murphy, R. M. Birn, and P. A. Bandettini, NeuroImage **80**, 349 (2013).
[123] A. A. Hagberg, D. A. Schult, and P. J. Swart, Exploring network structure, dynamics, and function using networkX, in *Proceedings of the 7th Python in Science Conference (SciPy2008), Pasadena, California*, edited by G. Varoquaux, T. Vaught, and J. Millman (2008), pp. 11–15.
[124] I. M. Bomze, M. Budinich, and P. M. Pardalos, The maximum clique problem, in *Handbook of Combinatorial Optimization*, edited by D.-Z. Du and P. M. Pardalos (Kluwer, Dordrecht, 1999), p. 1.
[125] T. E. Oliphant, *Guide to NumPy* (Continuum Press, Austin, TS, 2015).